Estimation of surface elevation changes at bare earth riverbank using differential DEM technique of UAV imagery data

Norhafizi Mohamad[1], Anuar Ahmad[1], Ami Hassan Md Din[2,3]

[1]Geomatics Innovation Research Group (GnG), Faculty of Built Environment and Surveying, Universiti Teknologi Malaysia, 81310 Skudai, Malaysia.
[2]Geospatial Imaging and Information Research Group (GI2RG), Faculty of Built Environment and Surveying, Universiti Teknologi Malaysia, 81310 Skudai, Malaysia.
[3]Geoscience and Digital Earth Centre (INSTeG), Faculty of Built Environment and Surveying, Universiti Teknologi Malaysia, 81310 Skudai, Malaysia.

Correspondence: Norhafizi Mohamad (email: norhafizi3@graduate.utm.my)

Received: 02 August 2021; Accepted: 01 September 2021; Published: 30 November 2021

Abstract

Estimating surface elevation changes at bare earth riverbank is challenging because of the non-visibility effect of this phenomenon, especially for short observation periods. Hence, the spatio-temporal detection at a short-term period determines the geomorphological changes by comparing the same area at different observation epochs. This study attempts to assess surface elevation changes components which include erosion and accretion, using the geomorphological changes detection (GCD) technique based on multi-temporal unmanned aerial vehicle (UAV) imagery. Using a multi-rotor UAV and high accuracy Global Navigation Satellite System instrument, the data acquisition process was conducted in Kilim River in the December 2016 and December 2017 to complete a one-year interval. To generate a very high accuracy of orthomosaics and digital elevation model (DEM), the structured from motion and multi-view stereo techniques were used. Then, GCD method, which involves a difference of DEM (DoD) was performed to evaluate the surface elevation changes that comprising erosion and accretion using GCD analysis tool. This study discovered that surface raising was more dominant than surface lowering, at 31.70% (raw) and 31.67% (thresholded), the per cent elevation raising at 68.30% (raw) and 68.33% (thresholded), the per cent imbalance (departure from equilibrium) at 18.30% (raw) and 18.33% (thresholded) and the net to total volume ratio at 36.60% (raw) and 36.67% (thresholded). The results showed how the UAV platform provides a way to evaluate surface elevation changes in bare earth areas with decent accuracy and enables further study on river geomorphological-related issues in the future.

Keywords: DEM, GCD Analysis, GNSS, SfM-MVS, Surface Elevation Changes, UAV Photogrammetry

Introduction

The study of geomorphological changes and riverbank erosion has got attention from researchers all around the globe. Geomorphology is a field of study related to the earth's surface, which encompasses the landforms, processes acting upon these landforms, and development (Corenblit et al., 2011; Li et al., 2017). Geomorphological processes occur due to the trigger factor, such as moving water, ice, wind and waves (Gardner, 2020). The sediment transport and discharge create the equilibrium at the riverbank structure, which forms a geomorphological-related process, such as fluvial erosion and slope failure. The long-term impact of this phenomenon could speed up the geomorphological changes and eventually affect the entire environment.

The real challenge in studying geomorphological changes and fluvial erosion is about the non-visible effect of these phenomena during the short-term period, especially when the observations periods are short. The recent development in computer vision such as structure from motion (SfM) and multi-view stereo (MVS) as well as image processing software has enhanced the capability of aerial photogrammetry to monitor geomorphological changes at small scale areas (Javernick et al., 2014; Lucieer et al., 2014; Smith et al., 2016; Koci et al., 2017; Mohamad et al., 2021). With the rapid growth in UAV technology, many researchers can own a low-cost UAV and able to perform data collection with low budget, low personnel, time saving and accurate output (Sorensen et al., 2017; Ventura et al., 2016). Besides, UAV has some advantages of flying at very low altitudes and could capture a very high-resolution image compared to conventional digital aerial image from airborne.

In this study, an attempt to monitor the geomorphological changes at Kilim River, Langkawi, Kedah, Malaysia has been made using multi-temporal UAV imagery, which was processed using SfM-MVS algorithms and incorporated with high ground control point's (GCP's) accuracy, observed from Global Navigation Satellite System (GNSS) equipment. The comparison of geomorphological features at a one-year period of digital elevation model (DEM) was carried out using the geomorphological changes detection (GCD) technique and volumetric changes at certain selected mark locations at Kilim River. Flying UAVs at low altitudes is the best method to evaluate Kilim River changes in a short-term period and detect even the tiny alteration (centimetres-scale) of earth surfaces because of natural or man-made factors.

Data and methodology

Study area

The study area was selected at Kilim River, in the north-eastern part of Langkawi Island, Kedah, Malaysia (see Figure 1). Kilim River is part of Kilim Karst Geoforest Park (KKGP), a geoforest park that was granted by the United Nations Educational, Scientific and Cultural Organization (UNESCO) in 2007 because of the impressive rock formations (i.e. limestone or karst), the richness of mangrove forest and the unique geological significance (Mohamad, 2019; Halim, 2019; Mohamad et al; 2020). Although most of the study area is covered by thick mangrove forest, there is still a bare area, especially at the riverbank, making this area suitable for this study.

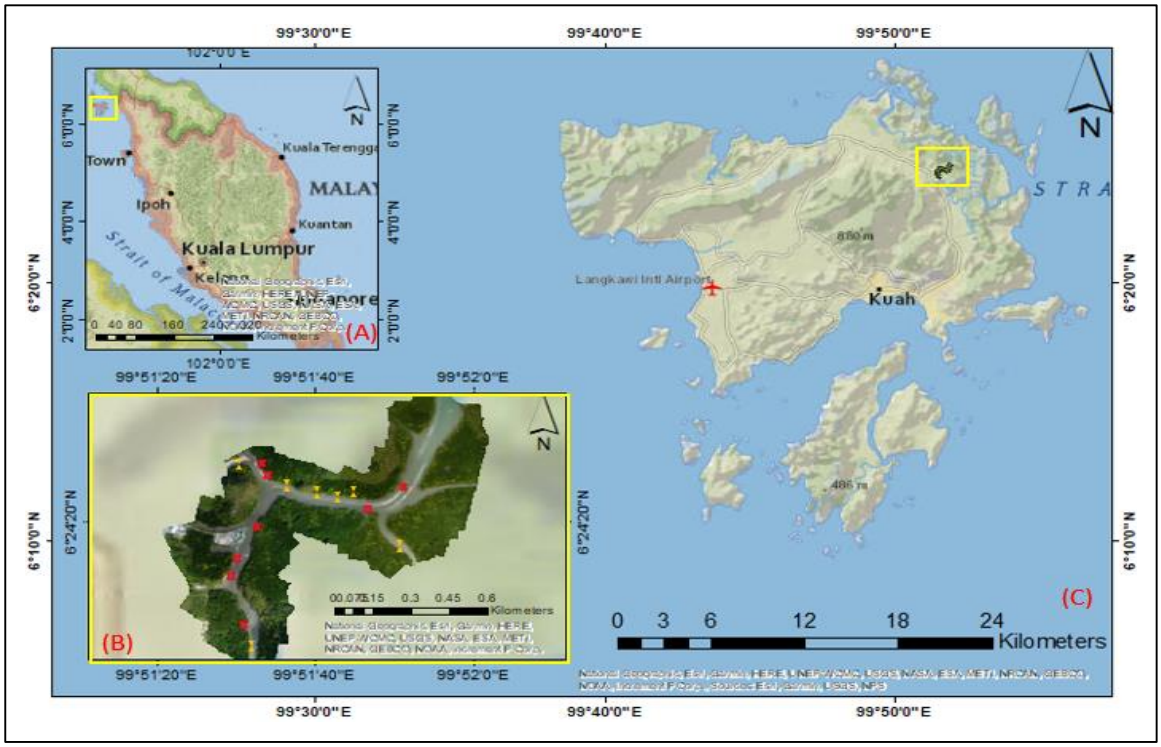

Figure 1. (A) Location of Langkawi Island from Peninsular Malaysia; (B) Orthomosaics image of Kilim River displaying the whole study area. (C); Area of interest (AOI) of Kilim River from aerial/satellite view.

Data

a. GNSS data for GCPs

GNSS measurement was carried out in December 2017. Eight GCPs were measured using Topcon GR-5 model, and the location was dispersed along the Kilim River, such as shown in Figure 1 (B). The static technique was chosen, and the measurement was referred to Continuously Operating Reference Station (CORS) at Langkawi and Arau station. Geocentric Datum of Malaysia 2000 (GDM 2000) as the geodetic datum and geoidal height for vertical datum was used to produce UAV output with vertical accuracy closest to the Mean Sea Level (MSL) value.

b. UAV photogrammetry data

UAV data were collected at Kilim River in December 2016 and 2017. Both epochs of data collection were carried out at low and high tide using the DJI Phantom 4 Advanced model. Epoch 1 was carried out on 5 December 2016 during high tide, while epoch 2 was conducted on 20 December 2017 during low tide conditions. DJI Phantom 4 Advanced model captured the images of Kilim River at the altitude of 149 m during epoch 1 while 228 m was the average altitude during epoch 2 (Figure 2). DJI GO software was used to plot the flight path and for planning the entire UAV data acquisition. 382 images were captured at epoch 1 and 116 images were captured at epoch 2 to cover the entire study area. The SfM-MVS process has produced orthophoto with a 5.5 cm/pix spatial resolution at epoch 1 and 6.17 cm/pix at epoch 2, while for DEM data, both epochs displayed 12.3 cm (epoch 1) and 10.4 cm (epoch 2).

Methodology

a. SfM-MVS workflow

SfM-MVS algorithm was chosen to construct the three-dimensional (3D) structure from a series of overlapping images instead of the conventional photogrammetry technique. Since SfM-MVS was a computer-aided solution of mathematical algorithms and digital softcopy of photogrammetry-based that devoid any opto-mechanical hardware, it was chosen to generate UAV output such as orthophoto and DSM (Smith et al., 2016; Koci et al., 2017; Lucieer et al., 2014).

The images were processed using SfM-MVS commercial software named Agisoft Metashape v1.6.4. The process started with image loading and image alignments to detect the location of matching tie point features in each image (Figure 2). The following process required eight input markers coordinates containing GCP coordinates to be inserted for estimating precision and accuracy through the computation of root-mean-square-error (RMSE). Then, the software optimised the camera and image to refine camera parameters. The process continued to dense and point cloud construction, before continuing to the last process for generating DSM and orthophotos.

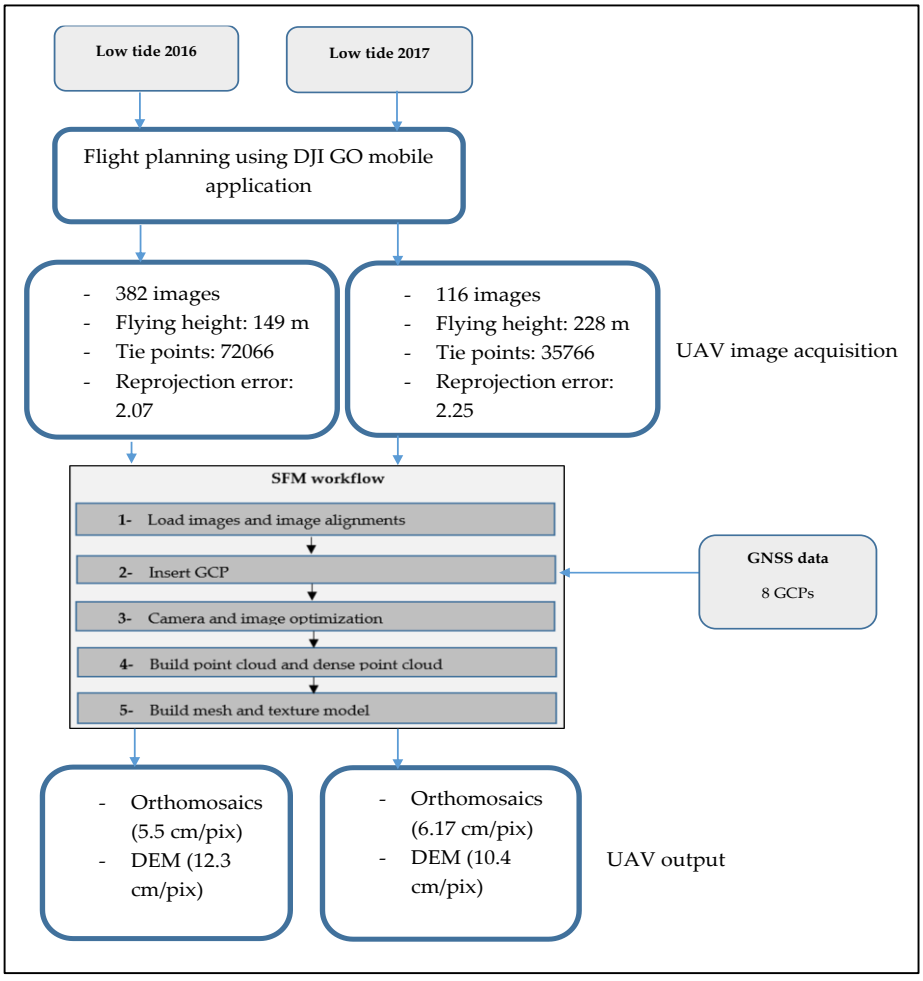

Figure 2. UAV data processing using the SfM-MVS method.

b. Geomorphological changes detection (GCD) workflow

The filtered DEM went through GCD-based processing using a geographical information system (GIS) tool that works within the ESRI ArcGIS Desktop. Using this method, volumetric changes volume was calculated based on surface elevation difference from UAV-derived DEMs from a repeated topographic survey (Vericat et al., 2017). Since DEM has an uncertain surface elevation due to space and time possibility errors, volumetric changes volume depends on each DEM's surface representation uncertainties, such as shown in Equation (1), to detect any surface elevation changes (Wheaton et al., 2010).

$$DoD = DEM_{t2} - DEM_{t1} \quad (1)$$

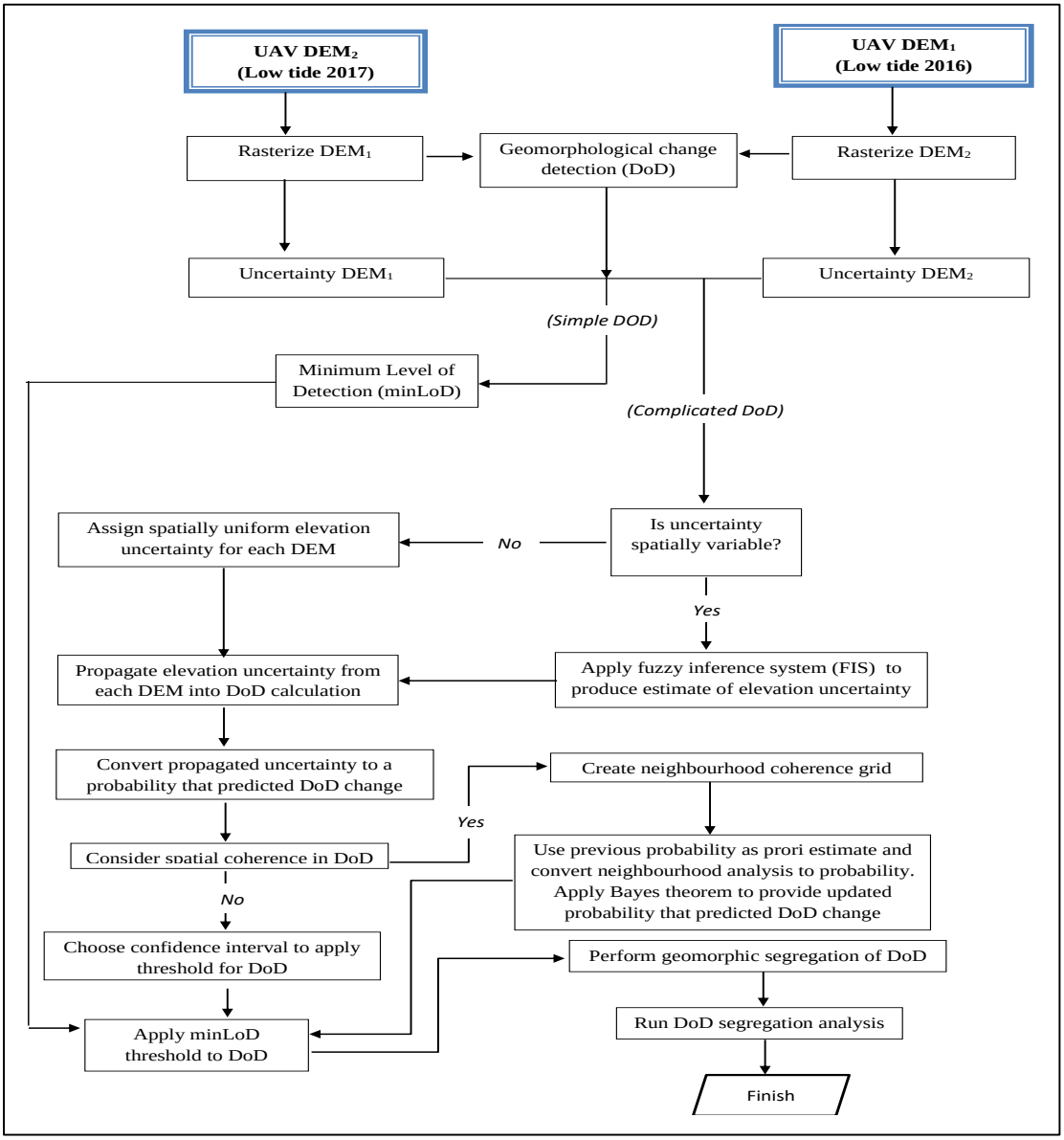

Figure 3. Change detection process at bare earth surface using GCD method.

GCD steps are displayed in Figure 3. First, GCD process started with vertical differences between two UAV-derived DEMs, followed by a non-parametric signed-rank test for DoD probabilistic assessment. Then, geomorphological surface feature extraction was carried out for slope variability analysis in each DEM grid cell. The variability of DoD comprises two situations; simple and complicated. A minimum level of detection (minLoD) should be applied for simple DoD uncertainty, while for complicated DoD uncertainty, spatial variability should be decided (Torresani et al., 2019). If there is no spatial variability, spatially uniform elevation uncertainty for each DEM should be assigned to propagate into DoD calculation. While if there is spatial variability, the fuzzy inference system (FIS) should produce elevation uncertainty estimation (Torresani et al., 2019).

Results and discussion

GNSS assessment for GCPs

This section summarised the GCP error for each epoch in 2016 and 2017 at low tide. For low tide observations in 2016 (Table 1), 7 GCPs were utilised, with the North (N) error being 1.37621 cm, the East (E) error being 1.0028 cm, the Orthometric height (H) error being 0.263027 cm, the North-East (NE) error being 1.70281 cm, and the overall error being 1.723 cm. Meanwhile, the low tide observation in 2017 shows that the N error was 1.30913 cm, the E error was 1.463104 cm, the H error was 0.23157 cm, the NE error was 1.9205 cm, and the overall error was 1.547 for all 8 GCPs in Table 2.

Table 1. GCP error for low tide (2016) data.

GCP	N error (cm)	E error (cm)	H error (cm)	NE error (cm)	Total (cm)
Station 4	-0.89777	-1.19112	0.234664	1.50991	0.089(41)
Station 6	-0.306796	0.0538895	-0.0711948	0.319526	0.297 (19)
Station 8	-1.4657	2.26345	-0.358834	2.72034	0.072 (50)
Station 9	2.476	-0.432766	0.461233	2.55551	0.227 (57)
Station 10	-1.93241	-0.536063	-0.277168	2.02445	0.258 (45)
Station 11	0.540469	-0.138552	0.0683863	0.562121	0.111 (22)
Station 12	-0.228695	-0.0230535	-0.0339218	0.232344	0.076 (41)
Total	1.37621	1.0028	0.263027	1.70281	1.723

Table 2. GCP error for low tide (2017) data.

GCP	N error (cm)	E error (cm)	H error (cm)	NE error (cm)	Total (cm)
Station 3	0.0488	-1.6137	0.43898	1.3361	0.17 (22)
Station 4	-0.306796	1.1734	1.712	2.3464	0.376 (20)
Station 6	0.915417	0.321744	0.53139	0.58065	0.085 (12)
Station 8	-1.24656	-0.71607	-1.9807	-1.1796	0.703 (21)
Station 9	1.51055	2.76164	-0.54751	-1.14202	0.025 (11)
Station 10	1.55624	-1.06974	0.18573	-1.42974	0.037 (7)
Station 11	-0.752021	0.42625	0.17605	0.47413	0.056 (20)
Station 12	-0.4165	0.17958	0.71563	0.19499	0.095 (23)
Total	1.30913	1.463104	0.23157	1.9205	1.547

Later that, all epochs were examined for error statistics in establishing the accuracy of the vertical component of UAV-derived DSM. The vertical component was calculated using orthometric height and was analysed to determine the minimum error (min), maximum error (max), mean error (ME), and standard deviation error (SDE). Table 3 shows the minimum error at 0.339 mm, the maximum error at 2.612 mm, the ME error at 1.697 mm, and the SDE error at 0.686 mm for low tide observations in 2016. Meanwhile, the minimum error for low tide observations in 2017 was -0.131 mm, the maximum error was 2.372 mm, the ME error was 1.660 mm, and the SDE error was 0.872 mm.

Table 3. GCP error for low tide (2017) data.

	2016 (Low tide)	**2017 (Low tide)**
Number of GCP (n)	7	8
Min (mm)	0.339	-0.131
Max (mm)	2.612	2.372
ME (mm)	1.697	1.660
SDE error (mm)	0.686	0.652

UAV outputs

Figure 4 depicted UAV output with orthomosaic and DSM data from two distinct epochs, 2016 and 2017. At DSM, the size for low tide (2016) was 17191 × 13529, whereas the size for low tide (2017) was 15810 x 13221. In 2016, the DSM height ranged from -99.8065 to 106.325 m, while the DSM height ranged from -93.9257 to 105.059 m. For orthomosaic and DSM data, the same WGS 84 (EPSG:4326) was utilised for all epochs, as shown in Figure 4. The orthomosaic photo at low tide 2016 seems to have a coverage area of around 0.661 km^2, but the orthomosaic photo in low tide 2017 had a larger coverage area of 0.688 km^2 along the whole Kilim River. The ground resolution during the low tide period in 2016 was 5.5 cm/pix, whereas it was 6.17 cm/pix in 2017. In terms of tie points, the low tide in 2016 was 72,066, while the high tide in 2017 was 35,766. In 2016, the projected low tides phase was 251,023, whereas in 2017, the projected low tides phase was 100,270. Meanwhile, the reprojection error for low tides in 2016 was 2.07, whereas it was 2.25 in 2017. In 2016, the orthomosaic size was 21756 x 19274 and 21484 x 19152, whereas in 2017, the size was 19892 x 19860 and 24438 x 23740.

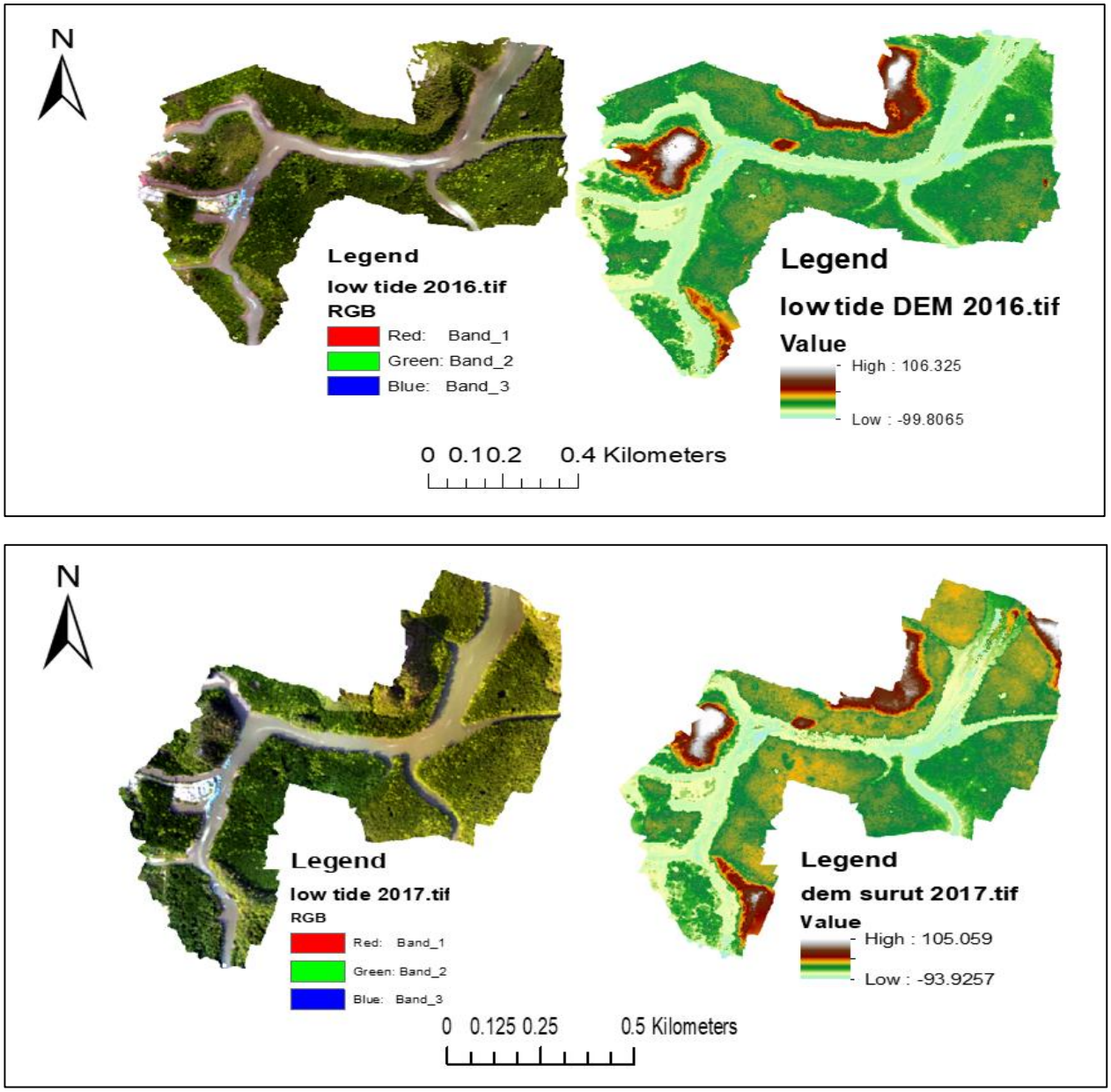

Figure 4. UAV output result using SfM-MVS method; (Top figure: Orthophoto and DSM result during low tide in 2016); (Bottom figure: Orthophoto and DSM result during low tide in 2017).

Change detection of DEM temporal data

The changes in surface elevation have been visualised at low tide in 2016 and 2017 in Figure 5. For one year epoch that the UAV observed, the area shows a significant change in surface lowering and raising. By implying the GCD method using the ArcGIS platform, change detection has been detected using a 0.20 m minimum level of detection (minLoD). The imbalance of surface lowering and raising, especially at the riverbank area through a percentage (by volume) analysis, was tabulated in Table 4. The table showed the percent elevation lowering at 31.70% (raw) and 31.67%

(thresholded), the percent elevation raising at 68.30% (raw) and 68.3% (thresholded), the percent imbalance (departure from equilibrium) at 18.30% (raw) and 18.33% (thresholded) and the net to total volume ratio at 36.60% (raw) and 36.67% (thresholded).

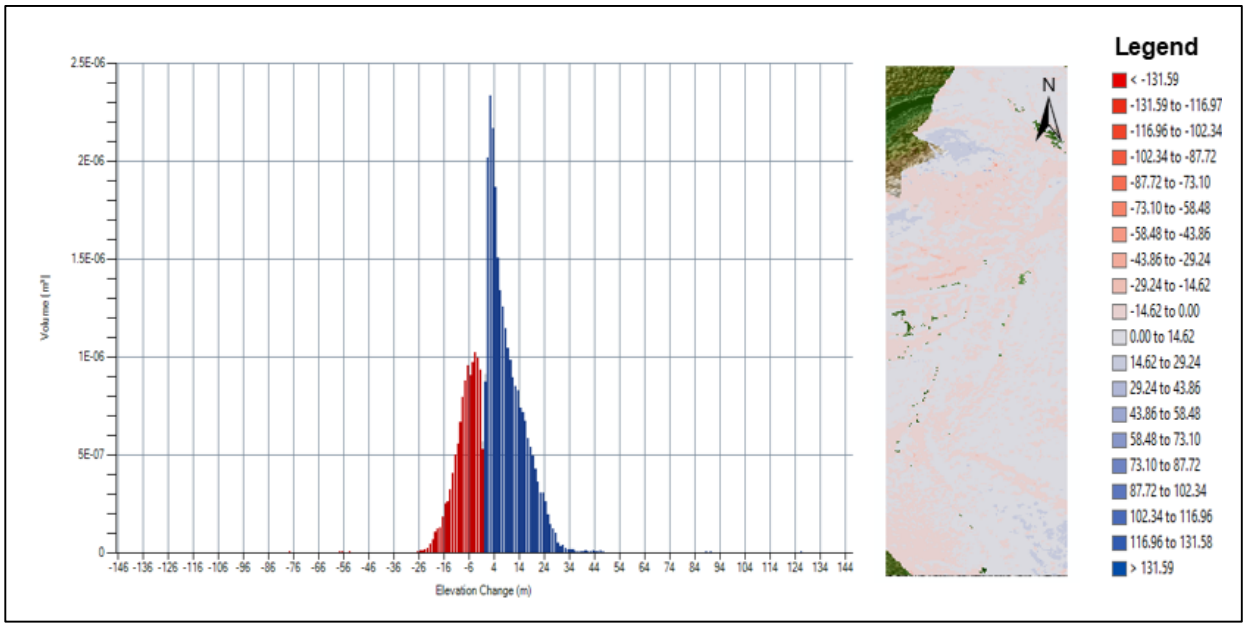

Figure 5. Change detection of the bare earth surface in Kilim River area using GCD method; (Left: Graphical results); (Middle: Change detection pattern); (Right: Elevation difference).

a. Volumetric Changes

Volumetric changes volume was calculated based on surface elevation difference from UAV-derived DEMs. In Figure 6, the left figure showed the total volume lowering and raising and the total net volume difference. Table 4 exhibited the percentage error of total surface lowering at 5.67%, the percentage error of total surface raising at 5%, the total percentage error of difference at 5.21% and the total net volume difference at 10.53%. The error percentage match well with Figure 6 (top figure) that display total volume of lowering at -0.0473687714 m^3, total volume of raising at 0.0165830369 m^3 and total net volume difference at 0.0060641523 m^3. These changes showed that elevation differences were more dominant on surface raising than surface lowering at the difference of 0.00606641523 m^3.

b. Areal Changes

Areal changes were quantified based on DEMs surface changes from the repeat topographic survey. In Figure 6, the middle figure showed the total lowering and raising's area. Meanwhile, Table 4 exhibited the total surface lowering's area, the total area of surface raising, the total detectable changes area, and the total interest area at 0.00 and NA value, but the per cent area of interest with detectable change is 92.30% at thresholded. The error percentage match well with Figure 6 (top figure) that display total area of lowering at -0.0173512652 m^2 and the total area of raising at 0.0347025308 m^2. These changes showed that 0.0173512656 m^2 of area was the difference between a total area of lowering and raising.

c. Vertical Averages

Vertical averages were calculated from differential DEMs vertical elevation derived from the repetitive UAV survey (Equation 1). In Figure 6, the right figure showed the average depth of volume lowering and raising as well as the average total thickness difference. Table 4 displays the average depth of surface lowering at 3.17 m (raw), 3.53 m (thresholded), ±0.20 m (error volume) and 5.67% (% error). Meanwhile, the average depth of surface raising showed 3.76 (raw), 4.00 (thresholded), ±0.20 (error volume) and 5.00 (% error). Subsequently, the average total thickness (m) for an area of interest recorded 3.55 (raw), 3.54 (thresholded), ±0.18 (error volume), and 5.21 (% error). For the average net thickness of difference (m) for an area of interest, the table displayed 1.30 (raw), 1.30 (thresholded), ±0.14 (error volume) and 10.52 (% error). Next, the average total thickness of difference in the area with detectable changes is NA (raw), 3,84 (thresholded), ±0.20 (error volume) and 5.21 (% error). Last, the average net thickness of the difference in the area with detectable changes showed NA (raw), 1.41 (thresholded), ±0.15 (error volume) and 10.52 (% error).

Table 4. Tabular results of surface elevation changes at Kilim River.

	Raw	Thresholded	Error Volume	% Error
Volumetric Changes				
Total volume of surface lowering (m^3)	0.0	0.0	±0.0	5.67
Total volume of surface raising (m^3)	0.0	0.0	±0.0	5.00
Total volume of difference (m^3)	0.0	0.0	±0.0	5.21
Total net volume difference (m^3)	0.0	0.0	±0.0	10.52
Areal Changes				
Total area of surface lowering (m^2)	0.00	0.00		
Total area of surface raising (m^2)	0.00	0.00		
Total area of detectable changes (m^2)	NA	0.00		
Total area of interest (m^2)	0.00	NA		
Percent area of interest with detectable change (m^2)	NA	92.30		
Vertical Averages				
Average depth of surface lowering	3.17	3.53	±0.20	5.67
Average depth of surface raising	3.76	4.00	±0.20	5.00
Average total thickness (m) for area of interest	3.55	3.54	±0.18	5.21
Average net thickness of difference (m) for area of interest	1.30	1.30	±0.14	10.52
Average total thickness of difference for area with detectable changes	NA	3.84	±0.20	5.21
Average net thickness of difference for area with detectable changes	NA	1.41	±0.15	10.52
Percentages (By Volume)				
Percent elevation lowering	31.70	31.67		
Percent elevation raising	68.30	68.33		
Percent imbalance (departure from equilibrium)	18.30	18.33		
Net to total volume ration	36.60	36.67		

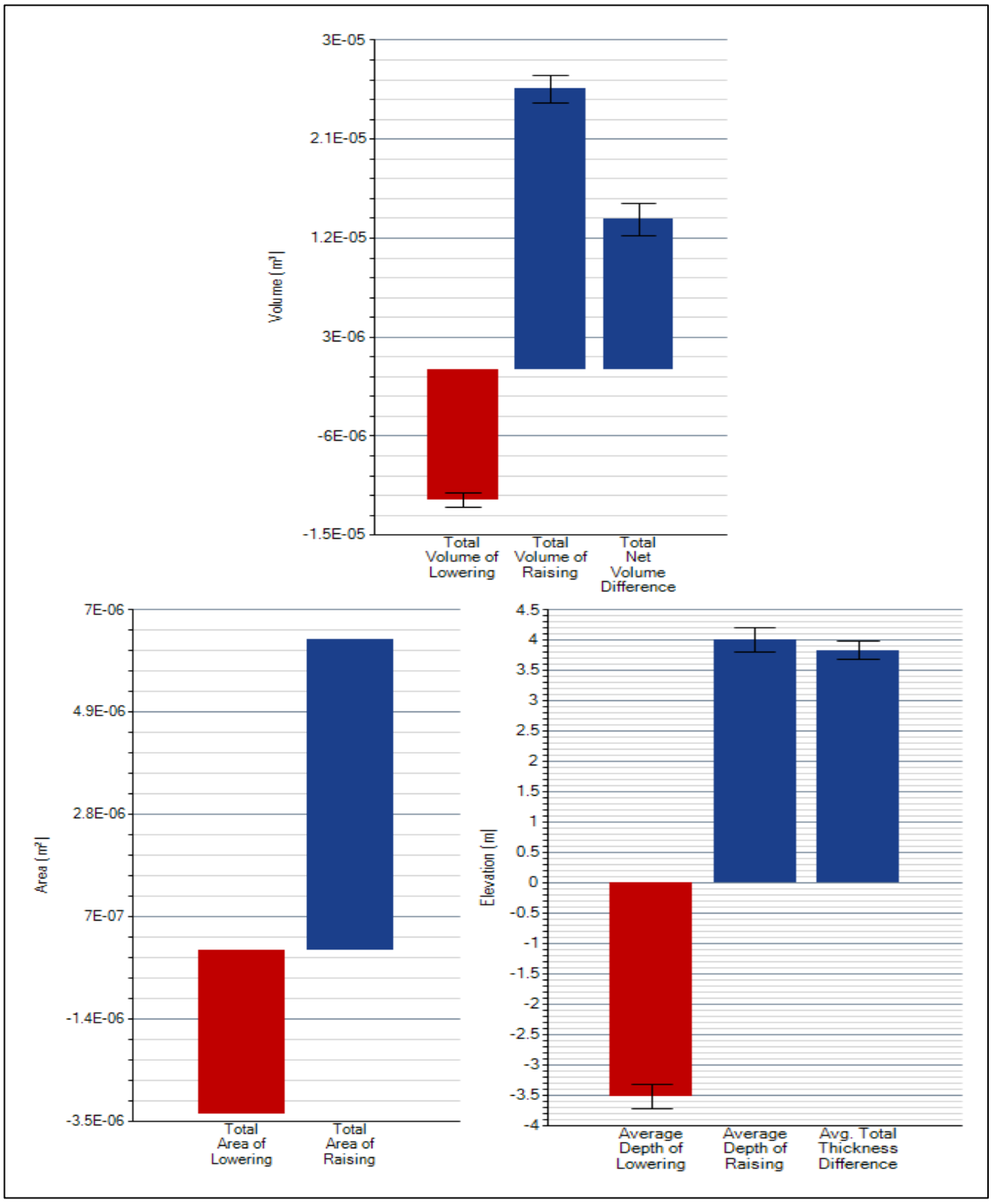

Figure 6. Surface elevation changes at bare earth area in Kilim River; (Top: Volumetric changes); (Bottom left: Areal changes); (Bottom right: Vertical averages).

Discussion

In order to thresholding the differential of the DEM (DoD) process and analyse the uncertainty of the surface, GCD method at 0.20 m minimum level of detection (minLoD) was utilised instead of propagated and probabilistic thresholding. Change detection results using the GCD method in Figure 4 has revealed the imbalance of surface lowering and raising at 31.70% (raw) and 31.67% (thresholded), the per cent elevation raising at 68.30% (raw) and 68.33% (thresholded), the per cent imbalance (departure from equilibrium) at 18.30% (raw) and 18.33% (thresholded) and the net to total volume ratio at 36.60% (raw) and 36.67% (thresholded).

Figures 5 and 6 were generated using GCD add-in tools in ArcGIS v10.4.1. In Figure 5, change detection patterns were discovered upon utilising two epochs of DEM data at one-year period, which seems that total surface raising was slightly dominant than surface lowering. In Figure 6, change detection results were segregated into three categories; volumetric changes, actual changes and vertical averages. These categories recorded significant changes more on surface raising rather than surface lowering. This situation hinted at the sub-surface movement, land subsidence, hydrology and geomorphological condition that experienced positive gaining of the surface because of a natural or anthropological phenomenon surrounding this area (Mohamad et al., 2020). Micro-seismic activities that frequently happen on the surface have increased the elevation at mm level for long-term changes, while man-made activities such as land reclamation in the riverbank area also affect the surface changes.

For surface lowering, the factor was known as riverbank erosion. According to the previous study by Mohamad (2019) and Mohamad et al., (2020), the riverbank along Kilim River had experienced a severe erosion problem because of multiple factors such as boat wakes and development activities. Halim (2019) also proved this phenomenon as part of threat that affects the beauty of this area that was granted Geopark status since 2007 and he also discovered that this area was developed as the eco-tourism hub part of mangrove forests were logged for this purpose. Hence, these previous studies had supported the existence of surface lowering because of erosion and human development.

Conclusion

In conclusion, an integration between UAV imagery and GNSS data allows user to estimate the surface elevation changes on bare earth. GCD add-in tools were integrated into commercial GIS software (ArcGIS) to analyse change detection among UAV-DEM data at two different epochs of observation to facilitate this process. The finding in this study concluded that the imbalance of surface elevation changes existed at the Kilim River with surface raising was slightly dominant compared to surface lowering. This condition happened because of natural or anthropological phenomena such as riverbank erosion, land reclamation and human development along the Kilim River. This study could enrich the understanding of UAV applications for evaluating the surface elevation changes in bare earth area with great accuracy and enable further study of river geomorphological-related issues in the future.

Acknowledgement

Much appreciation to the Universiti Teknologi Malaysia for providing financial aid to conduct this study through UTM High Impact Research (UTM HR), Vote Number: Q.J130000.2452.09G29. The authors also acknowledge the person that provides ideas and theory, sharing processing equipment, and giving technical support for this paper.

References

Corenblit, D., Baas, A.C., Bornette, G., Darrozes, J., Delmotte, S., Francis, R.A., Gurnell, A.M., Julien, F., Naiman, R.J., & Steiger, J. (2011). Feedbacks between geomorphology and biota controlling Earth surface processes and landforms: a review of foundation concepts and current understandings. *Earth Science Reviews, 106,* 307-331. https://doi.org/10.1016/j.earscirev.2011.03.002

Gardner, J. (2020). How water, wind, waves and ice shape landscapes and landforms: Historical contributions to geomorphic science. *Geomorphology, 366,* 106687. https://doi.org/10.1016/j.geomorph.2019.02.031

Halim, M.K.A. (2019). *Pemantauan Status dan Perubahan Bakau di Kilim, Langkawi Menggunakan Teknologi Penderiaan Jauh dan Sistem Maklumat Geografi* (Master dissertation). Retrieved from Faculty of Built Environment & Surveying, Universiti Teknologi Malaysia.

Javernick, L., Brasington., & Caruso, B. (2014). Modelling the topography of shallow braided rivers using Structure-from-Motion photogrammetry. *Geomorphology, 213*, 166-182. https://doi.org/10.1016/j.geomorph.2014.01.006

Koci, J., Jarihani, B., Leon, J.X., Sidle, R.C., Wilkinson, S. N., & Bartley, R. (2017). Assessment of UAV and ground-based structure from motion with multi-view stereo photogrammetry in a gullied savanna catchment. *ISPRS International Journal of Geo-Information*, *6*(11), 328. https://doi.org/10.3390/ijgi6110328

Li, J., Yang, L., Pu, R., & Liu, Y. (2017). A review on anthropogenic geomorphology. *Journal of Geographical Science*, *27*(1), 109-128. https://doi.org/10.1007/s11442-017-1367-7

Lucieer, A., Jong, S. M. D., & Turner, D. (2014). Mapping landslide displacements using Structure from Motion (SfM) and image correlation of multi-temporal UAV photography. *Progress in physical geography*, *38*(1), 97-116. https://doi.org/10.1177%2F0309133313515293

Mohamad, N. (2019). *Evaluation of Riverbank Erosion Based on Mangrove Boundary Changes Identification Using Multi Temporal Satellite Imagery.* (Master Dissertation). Retrieved from Faculty of Built Environment & Surveying, Universiti Teknologi Malaysia.

Mohamad, N., Ahmad, A., & Din, A.H.M. (2020). Monitoring Groundwater Depletion Due to Drought using Satellite Gravimetry: A Review. *Journal of Physic: IOP Conference Series,* 540, 012054. http://dx.doi.org/10.1088/1755-1315/540/1/012054

Mohamad, N., Ahmad, A. & Din, A.H.M. (2021). Derivation of MSL Riverbank Line from UAV DSM Data based on Tidal Slope Analysis. *Journal of Physic: IOP Conference Series*, 767, 012017. http://dx.doi.org/10.1088/1755-1315/767/1/012017

Smith, M.W., Carrivick, J.L., & Quincey, D.J. (2016). Structure from motion photogrammetry in physical geography. *Progress in Physical Geography,* 40(2), 247-275. https://doi.org/10.1177%2F0309133315615805

Sørensen, L.Y., Jacobsen, L.T. and Hansen, J.P. (2017). Low cost and flexible UAV deployment of sensors. *Sensors*, 17(1), 154. https://doi.org/10.3390/s17010154

Torresani, L., Wu, J., Masin, R., Penasa, M., & Tarolli, P. (2019). Estimating soil degradation in montane grasslands of North- eastern Italian Alps (Italy). *Heliyon*, 5(6), 01825. https://doi.org/10.1016/j.heliyon.2019.e01825

Ventura, D., Bruno, M., Lasinio, G. J., Belluscio, A., & Ardizzone, G. (2016). A low-cost drone based application for identifying and mapping of coastal fish nursery grounds. *Estuarine, Coastal and Shelf Science*, *171*, 85-98. https://doi.org/10.1016/j.ecss.2016.01.030

Vericat, D., Wheaton, J.M., & Brasington, J. (2017). Revisiting the morphological approach: opportunities and challenges with repeat high-resolution topography. *Gravel-Bed Rivers: Process and Disasters*, 121. https://doi.org/10.1002/9781118971437.ch5

Wheaton, J.M., Brasington, J., Darby, S.E., & Sear, D.A. (2010). Accounting for uncertainty in DEMs from repeat topographic surveys: improved sediment budgets. *Earth Surface Processes and Landforms*, 35(2), 136-156. https://doi.org/10.1002/esp.1886